HHS Public Access

Author manuscript

J Control Release. Author manuscript; available in PMC 2020 January 10.

Published in final edited form as:

J Control Release. 2019 January 10; 293: 1–9. doi:10.1016/j.jconrel.2018.10.033.

pH-Sensitive Morphological Transitions in Polymeric Tadpole Assemblies for Programmed Tumor Therapy

Cunfeng Song[a], **Tongtong Lin**[a], **Qiang Zhang**[a], **S. Thayumanavan**[b], and **Lei Ren**[a]

[a]State Key Lab of Physical Chemistry of Solid Surface, Key Laboratory of Biomedical Engineering of Fujian Province, Department of Biomaterials, College of Materials, Xiamen University, Xiamen 361005, China

[b]Department of Chemistry, University of Massachusetts, Amherst, MA 01003, USA

Abstract

Ultrafine single-chain tadpole polymers (SCTPs), containing an intrachain cross linked globule and a pH-sensitive linear polymer chain, have been synthesized. Self-assembly of these polymers depends on the linear block length and the pH, at which the polymer is assembled. Although the SCTPs themselves exhibit a size that is consistent with a single-chain species, the self-assembled SCTPs were found to be substantially larger. Since the transition between these two structures is reversibly dependent on pH, we explored the possibility of utilizing these assemblies to achieve deep tissue penetration in tumors. Our results indicate that there is indeed a pH-dependent deep tissue penetration in *ex vivo* tumor multicellular spheroids. Moreover, the multi-tadpole assemblies (MTAs) can stably encapsulate hydrophobic molecules, which has been used to encapsulate paclitaxel (PTX). These PTX/MTAs show excellent therapeutic efficacy and biosafety in 4T1 xeno graft mouse models. The innovative multi-compartment aggregates are able to fulfill structure-related function transitions with the variation of microenvironment, which has potential to extremely enrich the design of sophisticated biological agents.

Graphical abstract

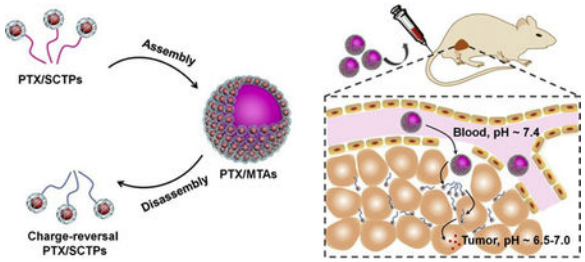

Keywords

antitumor agents; drug delivery; pH response; single-chain tadpole polymers; tumor penetration

1. Introduction

Cross-linking of a single polymer chain has attracted much attention, as it mimics the delicate controlled folding process of proteins to form well-defined morphologies.[1,2] According to the sequences of programmed monomer, a variety of conformationally diverse macromolecules (e.g., letter-shaped rings, globular single chain) have been generated by intrachain covalent, dynamic covalent, and non-covalent interactions.[3–8] Among them, single-chain tadpole polymers (SCTPs) with a crosslinked globule and linear tail, are capable of self-assembling into regular superstructures due to their anisotropy.[9–11] These multi-tadpole assemblies (MTAs) allow one to integrate discrete motifs into closely located nanospaces. Assembling SCTPs into well-defined structures are woefully under-explored. Fairly limited reports, which studied the assembly of SCTPs, mainly focus on assembling these macromolecules in organic solvents.[12,13] Studying this multi-compartment structure in water, would be of great interest,[14,15] as it allows for sequestering guest molecules into each functional motif. Furthermore, the MTAs are expected to make specific responses to tumor-associated stimulus and achieve the transition between their two structures, which can be used as drug carriers in tumor therapy.

Generally, large nanoparticles are suitable for prolonged blood circulation and preferential tumor accumulation through the enhanced permeability and retention (EPR) effect.[16–18] However, the intratumoral high interstitial fluid pressure, heterogeneous vasculature, and dense extracellular matrix make them difficult to penetrate into solid tumor, which directly leads to the insufficient release of anticancer drugs in the deep tumor tissue.[19] Small nanoparticles (~10 nm) are characterized with good intratumoral penetration effect,[20,21] but can be rapidly cleared out of the body before arrive at the tumor site.[22,23] Thus, in the past decades, nanocarriers, including traditional polymeric micelles, can hardly balance the accumulation and penetration in tumor because of their inherent architectures.[24–28]

Intelligent nanocarriers that undergo a large-to-small size change in the presence of the tumor-associated stimulus have gained much attention, for their potentials in solving these problems.[29] It is well known that the extracellular pH (pH_e) of solid tumor (~6.5–7.0) is more acidic than that of normal tissues and blood (~7.4).[30,31] Under the assistance of this characteristic, we presently report novel pH-sensitive SCTPs, where under one set of conditions, they aggregate to provide a larger, but well-defined, nanoassemblies in the stage of circulation and extravasation, where under a different set of conditions, they present themselves as single chain nano-objects to penetrate into the solid tumor (Scheme 1).

2. Materials and methods

2.1 Materials and characterization

4-Cyano-4-(phenylcarbonothioylthio) pentanoic acid (CPAD), OEGMA, DEA, DTT, DiI, DiO were purchased from Sigma-Aldrich (USA). PDS was synthesized according to our previous report.[32] The synthetic starting materials, and PTX were obtained from J&K (China). Fetal bovine serum (FBS) and RPMI 1640 medium were purchased from Biological Industries (USA). Hoechst 33258 and MTT were obtained from Beyotime (China). Milli-Q

water purified via the Milli-Q Plus System (Millipore, USA). All the used dialysis membranes (MWCO: 3500 Da) were obtained from Sangon Biotech (China).

^{1}H NMR spectra were recorded on a 400 MHz Bruker NMR spectrometer and calibrated against tetramethylsilane (TMS) standard. Dynamic light scattering (DLS) and zeta potential measurements were performed by a Malvern Nanozetasizer. The scattering intensity of nanoparticles were monitored by NanoBrook Omni. Gel permeation chromatography (GPC, Waters Acquity) was used to detect the molecular weight of polymers, using PMMA standard with a refractive index detector and DMF as the elution. Transmission electron microscopy (TEM) images were taken from JEM-2100 at 200 KV. The emission spectra were obtained from a Fluoromax-4 spectrofluorimeter.

2.2 Synthesis of PDEA-b-P(OEGMA-co-PDS)

CPAD (35 mg, 0.125 mmol), AIBN (8.2 mg, 0.5 mmol), and DEA (3.47 g, 18.75 mmol) were dissolved in dry THF (8 mL). The solution mixtures were subjected to five freeze-pump-thaw cycles and filled with argon. The sealed flask was immersed in a preheated oil bath at 65 °C for 12 h. After polymerization, the resultant mixture was dialyzed against methanol to remove unreactive monomers. For synthesis of PDEA2-PDEA3, CPAD (35 mg, 0.125 mmol), AIBN (8.2 mg, 0.1 mmol) and DEA (1.62 g, 8.75 mmol) or (0.69 g, 3.75 mmol) were dissolved in 4 or 1.5 mL of dry THF for the reaction.

PDEA1-PDEA3 (0.05 mmol), OEGMA (3 g, 6 mmol), PDS (0.51 g, 2 mmol) were dissolved in 8 mL dry THF and degassed by performing five freeze-pump-thaw cycles. The reaction mixture was sealed and then transferred into a preheated oil bath at 65 °C. The polymerization reaction was allowed to proceed for 16 h (to P1), 22 h (to P2), 26 h (to P3). The characteristic peaks of DEA, PDS and OEGMA moieties versus chain transfer agent (CPAD) moieties were used to calculate the ratios of the monomer incorporated in the copolymer.

2.3 Preparation of SCTPs and MTAs

P1–P3 (0.5 mg) were separately dissolved in 1 mL PB of pH 6.9. Subsequently, DTT (50 mol% compared to PDS moieties) was dropwise added under stirring. The crosslinking reaction was allowed to performed overnight to form SCTPs. After that, the SCTPs solution was dialyzed against PB of pH 7.4 to gain MTAs. For fluorescence labelling these nanoparticles, Cy5.5-PEG-SH (o.05 mg) was added to one milliliter of SCTPs1 solution and then stirred for 12 h to obtain $^{Cy5.5}$SCTPs. Similarly, the $^{Cy5.5}$MTAs were prepared by dialysis against PB of pH 7.4.

2.4 Fluorescence Resonance Energy Transfer (FRET) experiment

DiI or DiO (0.01 mg in acetone) was added to one milliliter of the stock solution of P1 (0.5 mg/mL) with stirring. A calculated amount of DTT (25 mol% and 50 mol% against PDS moieties, respectively) was dropwise added, respectively. The vial was left uncapped to get rid of the acetone. After stirring for 12 h, insoluble DiI and DiO were removed by filtration using a syringe filter unit (pore size 0.22 μm). A solution of SCTPs containing DiI (100 μL) was mixed with a solution of SCTPs containing DiO (100 μL) in a cuvette, and then PB (pH

6.9, 800 μL) was added to adjust the volume. The fluorescence intensity was collected at 450 nm excitation wavelength.

2.5 In vitro drug release study

PTX (0.5 mg in acetone) was added to 12 mL of the stock solution of P1 (0.5 mg/mL) with stirring. Afterward, DTT (50 mol% compared to PDS moieties) was dropwise added to prepare PTX/SCTPs. The solution, placing in a dialysis membrane, was concentrated to a quarter by using polyethylene glycol (M_n 20000) to take up water, and then dialyzed against PB of pH 7.4 to form PTX/MTAs. The PTX-loading content was determined by the high performance liquid chromatography (HPLC) equipped with a photodiode array detector. The mobile phase was an acetonitrile/water (45:55 (v/v)) co-solvent with a flow rate of 1.0 mL min^{-1}. The drug-loading percent (DL) and entrapment efficiency (EE) of PTX/MTAs were calculated by the following formulas:

$$\mathrm{DL}(\%) = \frac{\text{Weight of PTX in MTAs}}{\text{Weight of PTX-loaded MTAS}} \times 100\%$$

$$\mathrm{EE}(\%) = \frac{\text{Weight of PTX in MTAs}}{\text{Weight of PTX added}} \times 100\%$$

The *in vitro* PTX release were investigated in the release medium: 0.1 M PBS of pH 6.9 containing 0.2% (w/v) Tween 80 with 10 mM or 10 μM GSH. Briefly, 3 mL of PTX/MTAs concentrated solution, placed into a dialysis membrane, were firstly immersed into PBS of pH 6.9 for equilibrium. Then, the stock solution was re-suspended in 30 mL release medium. The release experiments were carried out in an incubator (IKA-C) under gentle stirring (100 rpm) at 37 °C. Samples from supernatant were withdrawn at determined intervals and replaced with an equal volume of fresh release medium. The detection wavelength of paclitaxel was 227 nm.

2.6 Penetration assay

Human glioblastoma U87MG cells were cultured in DMEM at 37 °C under 5% CO_2 to form multicellular tumor spheroids (MCTS).[33] The medium was separately adjusted to pH 6.9 and 7.4, followed by the addition of $^{Cy5.5}$MTAs with a final concentration of 0.1 mg mL^{-1}. After 4 h incubation, MCTS were extremely washed with PBS and monitored by Leica TCS SP5 CLSM Z-stack scanning. To analyze *ex vivo* penetration,[34] the tumors were collected from 4T1 tumor-bearing mice, when their average volume had reached 300–400 mm^3. Whole tumors were cultured *ex vivo* for 24 h with MTAs (0.5 mg/mL) in medium adjusted to pH 6.9 or pH 7.4. Frozen sections of tumors were harvested. The edge and inside area of each tumor section were imaged using Nikon biological microscope (Eclipse ci).

2.7 Cellular uptake and cytotoxicity

Murine breast cancer 4T1 cells were cultured in RPMI 1640 medium containing 10% FBS and 1% penicillin at 37 °C under 5% CO_2. 4T1 cells were seeded in a 6-well plate covered with glass at a density of 2×10^5 cells $well^{-1}$ for 24 h. The culture media were removed and

then replaced by serum-free medium containing the $^{Cy5.5}$MTAs with a final concentration of 0.1 mg mL^{-1} for incubation at pH 6.9 and 7.4, respectively. After washed with PBS three times, the cells were observed by CLSM and flow cytometry measurement (Beckman Coulter Cell Lab Quanta SC).

The cellular cytotoxicity was determined by MTT assay. 4T1 cells in RPMI 1640 were seeded in 96-well plates at a density of 5000 cells $well^{-1}$ for 12 h. Subsequently, all the culture media were separately replaced by 200 μL of serum-free medium containing serial dilutions of MTAs (0, 25, 50, 75, 100, and 125 μg mL^{-1}) at pH 6.9 and 7.4. After incubation for 24 h, 20 μL of MTT solution (5 mg mL^{-1}) was added to each well. The plates were incubated for an additional 4 h at 37 °C and then the medium was removed. The purple formazan crystals produced by live cells in each well were dissolved by the subsequent addition of 150 μL of DMSO for 30 min. The absorbance was recorded on Microplate Reader (Model 680, Bio-Rad Laboratories Richmond) at a set wavelength of 570 nm.

2.8 In vivo fluorescence imaging

Female BALB/c athymic nude mice 6–8 weeks of age were purchased from Shanghai SLRC Laboratories. To generate the tumor model, 4T1 cells (2×10^6) suspended in 100 μL PBS was subcutaneously injected into the flank of each mouse. 200 μL of $^{Cy5.5}$SCTPs and $^{Cy5.5}$MTAs was separately injected into caudal vein of each mouse. Afterward, the mice were imaged by an *in vivo* optical imaging system (IVIV Lumina II). The fluorescence detector was set at 675 nm for excitation and 695 nm for emission.

2.9 Antitumor efficacy

Female BALB/c mice 6–8 weeks of age were randomly divided into four groups (n=3 per group). When 4T1 tumor volumes reached about 100 mm^3, the treatment was started. Each reagent (PBS, PTX, PTX/SCTPs, or PTX/MTAs) was intravenously injected into the tail of mouse. The injection was carried out every 2 days for a total of four injections (PTX dose: 5 mg kg^{-1}). Tumor size of each mouse was measured by vernier caliper and the tumor volume (V) was estimated using the formula $V = (\text{length} \times \text{width}^2)/2$.

2.10 Histology examination

Tumors and the major organs of mice were harvested after treatment, fixed in 5% paraformaldehyde solution. After embedded into paraffin, they were sectioned into 5 μm thick slices. These slices were stained with H&E and then examined by a light microscopy.

3. Results and discussion

3.1 Design and synthesis of pH-sensitive SCTPs, and fabrication of their nanostructured assemblies

For our design, 2-(pyridydisulfide) ethyl methacrylate (PDS), oligoethyleneglycol methacrylate (OEGMA), and 2-(diethylamino)ethyl methacrylate (DEA) were utilized to synthesize copolymer PDEA-*b*-P(OEGMA-*co*-PDS) (Fig. S1). Folding/collapse of single polymer chain to form SCTP was driven by disulfide-induced intrachain crosslinking. We prepared three copolymers (**P1**-**P3**) with varying degrees of polymerization in DEA.

Increases in molecular weight from PDEA to PDEA-*b*-P(OEGMA-*co*-PDS) were observed in Figure S2a–c. The number-average molecular weights (M_n) and dispersity (M_w/M_n) of **P1**-**P3** were also analyzed by gel permeation chromatography (GPC) (Table 1). Then, **P1**-**P3** were converted into the corresponding nano-objects, **SCTPs1**-**SCTPs3**, by adding a predetermined amount of dithiothreitol (DTT) in THF. When 50 mol% of DTT against total PDS moieties was used in a dilute polymer solution, an equal amount of PDS groups were cleaved to generate free thiols. These thiol groups then react with the remaining PDS moieties within the single polymer chain to produce fully crosslinked nano-objects. Since intramolecular crosslinking will cause a necessary decrease in volume,[35,36] the volume changes between PDEA-*b*-P(OEGMA-*co*-PDS) and SCTP were monitored by GPC. Thereby, the observation of an increase in retention time can be taken to be an indicator of the formation of SCTP. Comparing with the corresponding copolymers, the retention times of all the crosslinked nano-objects were slightly prolonged (Fig. S2a–c). We also attempted to measure the change in hydrodynamic sizes (D_h) by using dynamic light scattering (DLS). It can be clearly observed that D_h of **SCTPs1**-**SCTPs3** became smaller than that of **P1**-**P3** (Fig. S2d–f).

Effect of the DEA units length on the self-assembly behavior of SCTPs was then investigated. To test the pH-triggered assembly, SCTPs were incubated in a series of phosphate buffer (PB) solutions with pH values in the range of 6.6 to 7.4, and their size changes were measured by DLS. There is a sharp transition from 9.6 ± 0.3 nm at pH 6.9 to 68.7 ± 2.8 nm at pH 7.0, indicating that **SCTPs1** is ultrasensitive to acidic environment (Fig. 1a). Moreover, the reversible size variation continuously occurred when pH alternately changed from below to above the critical transition value. As for **SCTPs2**, the transition pH value shifted to 7.2 (Fig. 1b). In contrast, **SCTPs3** maintained the initial state regardless of the variation of pH (Fig. 1c). These observations are understood, considering the factors that affect self-assembly. It is known that there needs to be a critical hydrophobic block length for self-assembly.[37,38] In addition, the relative hydrophilic-lipophilic balance (HLB) of the polymer can also dictate the self-assembly process. The former requirement is the possible reason for SCTPs3 not exhibiting any assembly. Moreover, as the pH decreases in the solution, a certain percentage of amine moieties will be protonated as one approaches their p*K*a. The critical percentage of functional groups that needs to be in the unprotonated state for self-assembly is likely to be dependent on the length of the pH-sensitive hydrophobic chain. This is the possible reason for the difference in the pH at which the size transition happens in **SCTPs1** *vs.* **SCTPs2**.

Due to the tumor pH-sensitivity, **SCTPs1** was chosen to prepare MTAs for the following studies. The morphological transition process of **SCTPs1** was followed by transmission electron microscopy (TEM). The ultrafine nano-objects were individually dispersed at pH 6.9 (Fig. 1d), with zeta-potential of 17.3 ± 0.9 mV. Subject to the pH of medium increasing to 7.4, **SCTPs1** could self-assemble into micelle-like MTAs (Fig. 1e). The deprotonated PDEA were hydrophobic and aggregated to form the core of the nanomicelle at pH above p*K*a.[39,40] The critical micelle concentration (CMC) of SCTPs can be investigated by DLS.[9] As shown in Fig. S3a, the scattering intensity of SCTPs1 was recorded when the concentration ranging from 0.001 to 0.5 mg/mL. The inflection point at CMC (0.047

mg/mL) indicated the formation of micellar assemblies. To confirm the disassembly of MTAs at the tumor acidity, the assemblies were incubated at pH 6.9 again. The protonation of PDEA blocks, which could be estimated by the variation of zeta-potential from -4.8 ± 0.3 mV to 16.7 ± 1.2 mV, led to the electrostatic repulsion between **SCTPs1.** Interestingly, the dissociation process of MTAs is observed by dialysis against PB solution (Fig. 1f). The complete dissociation of MTAs is presented in Fig. 1g. In addition, the time-dependent dissociation of MTAs was investigated by adding 1M HCl to adjust the pH of solution instantaneously. The abrupt decrease of scattering intensity proves that the size transition at acidic pH can be achieved within tens of seconds (Fig. S3b). According to this characteristic, **SCTPs1** can be employed to incorporate anticancer drug at low pH and then maintain their stability during blood circulation at physiological pH in the form of assemblies. After arriving at the tumor site, MTAs can dissociate instantaneously into SCTPs for penetrating the tissue.

3.2 Encapsulation stability and triggered release

We investigated the stability of encapsulation of guest molecules in each SCTP by Fluorescence Resonance Energy Transfer (FRET).[41] 3,3'-Dioctadecyloxacarbocyanine perchlorate (DiO) and 1,1'-dioctadecyl-3,3,3',3'-tetramethylindocarbocyanine perchlorate (DiI) are well-known as lipophilic FRET donor and acceptor pair, respectively. Two types of SCTPs solutions, one with DiO and another with Dil, were mixed. We excited the mixed solution at 450 nm, the wavelength at which DiO adsorbs. When there is a significant exchange of guest molecules, the extent of FRET will be enhanced with time. For these experiments, SCTPs with different crosslink densities were prepared by adding different amounts of DTT to **P1**. It is noteworthy that SCTPs-50 mol% DTT (that is **SCTPs1**) exhibit less leakage of sequestered dye molecules for 5 h, comparing with SCTPs-25 mol% DTT (Fig. S4). This result suggests that the stability of encapsulation of guest molecules is highly dependent on the crosslink densities of SCTPs.

Then, an anticancer drug, paclitaxel (PTX), was encapsulated into **SCTPs1** to obtain PTX/SCTPs (10.8 ± 0.2 nm), which assembled to obtain PTX/MTAs (76.9 ± 3.4 nm) (Fig. 2a and b). The PTX-drug loading percent (DL) and encapsulation efficiency (EE) of assemblies were determined as 5.6 ± 0.4% and 71.2 ± 5.2%, respectively. The stabilities of SCTPs and MTAs, with and without PTX, were respectively investigated in PB solution at pH 6.9 and pH 7.4. As shown in Fig. S5, the particle sizes exhibit no obvious change within 48 h. The electrostatic repulsion and hydrophilic interaction enable SCTPs to avoid aggregation at acidic pH. Combining with the results of the pH-dependent dissociation experiment above, MTAs should be stable, unless the change of pH happens. In addition, the encapsulation of PTX cannot affect the stability of both SCTPs and MTAs.

An effective nanocarrier should respond to a specific stimulus and then release drugs for therapy. In our system, besides inducing the intramolecular crosslinking, the disulfide bonds can be cleaved by high concentration of reducing agent (e.g., reduced glutathione (GSH), thioredoxin) in the cytosol.[42,43] To explore triggered release, we added different concentrations of GSH to PBS as release medium. It is obvious that the extent of PTX released from the nanocarriers showed a strong GSH dependence: when exposed to 10 mM

GSH, about 65% of loaded PTX were release at 48 h; while, less than 10% of loaded PTX were released in the presence of 10 μM GSH over 72 h (Fig. 2c). Therefore, this property can be conducive to facilitate intracellular delivery of encapsulated PTX.

3.3 Tumor Penetration, Cellular Uptake, and Cytotoxicity

U87MG multicellular tumor spheroids (MCTS) were used to assess the intratumoral penetration of MTAs at pH 6.9 and 7.4, respectively. After incubating with Cy5.5-labeled MTAs (denoted as $^{Cy5.5}$MTAs) for 4 h, MCTS were monitored by confocal laser scanning microscopy (CLSM) Z-stack scanning. The bottom of the MCTS was defined as 0 μm. At pH 7.4, the red fluorescence of Cy5.5 mostly located on the peripheral region of the MCTS (Fig. 3a). On the contrary, the fluorescence inside another MCTS was observed at each scanning depth, which indicates that the penetration capability has been significantly enhanced at acidic pH. Because of the protonation of PDEA blocks in the acidic milieu, electrostatic repulsion and the change in the HLB of the SCTPs induces the dissociation of MTAs into SCTPs. To further demonstrate this result, diffusion of MTAs into tumors was investigated by exposing them to excised cancer tissue in cell medium at pH 6.9 and 7.4, respectively. The images of the cryostat section clearly showed that the fluorescence within the tumor was homogeneous, as a result of MTAs disassembly at pH 6.9. Whereas, MTAs at pH 7.4 showed minimal penetration, since the fluorescence was mostly retained in the tumor edge (Fig. 3b). Consistent with the former reports,[44–46] the small size of the product SCTPs presumably enables nanoparticles to deeply penetrate and uniformly diffuse into tumor tissues.

To confirm the cellular uptake efficiency, murine breast cancer 4T1 cells were separately incubated with $^{Cy5.5}$MTAs at pH 6.9 and 7.4 for designed time. After incubation with $^{Cy5.5}$MTAs at acidic pH for 1 h, the strong red fluorescence was observed in cells (Fig. 4a). For 2 h and 4 h, the red signal from $^{Cy5.5}$MTAs treatment at pH 6.9 was much stronger than that from $^{Cy5.5}$MTAs treatment at pH 7.4. This phenomenon was also correlated with the disassembly of $^{Cy5.5}$MTAs in acidic milieu. Flow cytometry data also exhibited that the internalization of dissociated $^{Cy5.5}$MTAs was much faster and more efficient than that of $^{Cy5.5}$MTAs (Fig. 4b and c). These results are attributable to: i) Generally, positively charged nanocarriers tend to be taken up by cells, compared to neutral and negatively charged ones.[47,48] ii) Size-dependent endocytosis stimulates the intracellular uptake of smaller ones.[49] Furthermore, along with the extension of time, most red fluorescence located in cytosol containing high concentration of GSH, which stimulate the rapid release of the drug loaded by these nanocarriers.

For the former scenario, note that there have been reports that positively charged nano-objects exhibit significant toxicity.[50,51] To check if this is an issue here, the potential cytotoxicity of this delivery system was evaluated using 3-(4,5-dimethyl-thiazol-2-yl)-2,5-diphenyl tetrazolium bromide (MTT) assay on 4T1 cell line at two different pHs. The viabilities of the cells were above 90% after treatment with all tested concentrations of MTAs at pH 6.9 and 7.4, respectively (Fig. S6). Despite large-to-small size transition and weakly negative-to-positive charge transition exist, this system still displays an extremely low toxicity to cells.

3.4 Tumor Targeting, Antitumor Activity and Biosafety of MTAs

BALB/c nude mice bearing 4T1 exnografts after intravenous injection with $^{Cy5.5}$SCTPs and $^{Cy5.5}$MTAs were captured by an *in vivo* optical imaging system to evaluate the tumor-specific targeting capability. The strong fluorescence of Cy5.5 was observed in the liver organs in the first 1 h for both $^{Cy5.5}$SCTPs and $^{Cy5.5}$MTAs groups (Fig. 5a). During the testing process, the fluorescence signal of $^{Cy5.5}$SCTPs group did not appear at the tumor site, and the intensity in the whole body was decreased. The luminal surface of blood vessels possesses amounts of negatively charge resulting from sulfated and carboxylate sugar moieties.[52] Based on the previous reports,[53,54] when small SCTPs with high positive charges surface presented, they will bind nonspecifically to the luminal surface of vascular walls and be rapidly cleared from the blood circulation. In contrast, with the increase of circulation time, the stronger signals appeared at the tumor site for $^{Cy5.5}$MTAs group. The highest signal intensity in tumor was observed at 12 h post-injection. Owing to the effective EPR effect, MTAs are suitable for anticancer drug delivery to tumor through blood circulation.

The antitumor efficacy of PTX/MTAs was further investigated on the 4T1 tumor-bearing mice. All the mice were separately treated with PBS, PTX, PTX/SCTPs, and PTX/MTAs *via* the intravenous injection. The tumor growth curves and photographs of the excised tumors are displayed (Fig. 5b and c). In the group treated with PBS, the tumors grew rapidly over 1050 mm^3 within 14 days. Free PTX and PTX/SCTPs treatments (5 mg kg^{-1} of PTX equivalent) only slightly inhibited the tumor growth versus PBS treatment, which could be ascribed to the insufficient extravasation at the tumor sites. By contrast, 82% tumor suppression was observed in the group treated with PTX/MTAs. As a result of the effective cascade delivery, PTX/MTAs presented the superior tumor inhibition effect at a small dose. Hematoxylin and eosin (H&E) staining was used to estimate the cell apoptosis in tumor (Fig. 5d). The typically histologic characteristics of malignant tumors such as hyperchromatic nuclei and scant cytoplasm were observed in PBS group. In contrast, obvious nuclear shrinkage and fragmentation were found in the tumor slices of the other three-treated groups, especially for the one treated with PTX/MTAs.

Finally, the major organs from the mice after the treatment, including the heart, liver, spleen, lung and kidney, were further analyzed by histological examination. No organ was damaged in the four groups (Fig. 6), which verified that PTX/MTAs has no toxicity to living animals and could be used as a promising antitumor agent.

4. Conclusions

In summary, a new size-switchable delivery system has been developed based on ultrafine SCTPs with a disulfide-crossliked globule and linear PDEA blocks. Through the deprotonation of PDEA blocks, the SCTPs could self-assemble into larger micelle-like MTAs. The size-switchable delivery system, appearing in the initial form of MTAs at physiological pH, is beneficial to promote tumor accumulation. Once accumulated into acidic tumor microenvironment, MTAs dissociate into SCTPs. The small, positively charged SCTPs seem to be able to improve tumor penetration and cellular uptake efficiency. This biosafe system controllably releases the anticancer drug in response to intracellular stimulus, and inhibits the tumor growth efficiently. Overall, the pH-sensitive reversible morphological

transition in MTAs provides opportunities for an effective delivery cascade of anticancer drugs. Moreover, the strategy of polymeric multi-compartment structure can be adopted for designing smart biological agents.

Supplementary Material

Refer to Web version on PubMed Central for supplementary material.

Acknowledgements

This work was supported by the National Natural Science Foundation of China (U1505228, 31371012, 31870994), the China Postdoctoral Science Foundation (2016M602075), and Science Foundation of Fujian Province (2017Y0078).

References:

[1]. Ouchi M, Badi N, Lutz J-F, Sawamoto M, Single-chain technology using discrete synthetic macromolecules, Nat. Chem 3 (2011) 917–924. [PubMed: 22109270]

[2]. Gonzalez-Burgos M, Latorre-Sanchez A, Pomposo JA, Advances in single chain technology, Chem. Soc. Rev 44 (2015) 6122–6142. [PubMed: 26505056]

[3]. Schmidt BVKJ, Fechler N, Falkenhagen J, Lutz J-F, Controlled folding of synthetic polymer chains through the formation of positionable covalent bridges, Nat. Chem 3 (2011) 234–238. [PubMed: 21336330]

[4]. Lu J, ten Brummelhuis N, Weck M, Intramolecular folding of triblock copolymers via quadrupole interactions between poly(styrene) and poly(pentafluorostyrene) blocks, Chem. Commun 50 (2014) 6225–6227.

[5]. Jiang J, Thayumanavan S, Synthesis and characterization of amine-functionalized polystyrene nanoparticles, Macromolecules 38 (2005) 5886–5891.

[6]. Whitaker DE, Mahon CS, Fulton DA, Thermoresponsive dynamic covalent single-chain polymer nanoparticles reversibly transform into a hydrogel, Angew. Chem., Int. Ed 52 (2013) 956–959.

[7]. Song C, Li L, Dai L, Thayumanavan S, Responsive single-chain polymer nanoparticles with host–guest features, Polym. Chem 6 (2015) 4828–4834.

[8]. Cole JP, Lessard JJ, Rodriguez KJ, Hanlon AM, Reville EK, Mancinelli JP, Berda EB, Single-chain nanoparticles containing sequence-defined segments: using primary structure control to promote secondary and tertiary structures in synthetic protein mimics, Polym. Chem 8 (2017) 5829–5835.

[9]. Li W, Kuo C-H, Kanyo I, Thanneeru S, He J, Synthesis and self-assembly of amphiphilic hybrid nano building blocks via self-collapse of polymer single chains, Macromolecules 47 (2014) 5932–5941.

[10]. Wen J, Zhang J, Zhang Y, Yang Y, Zhao H, Controlled self-assembly of amphiphilic monotailed single-chain nanoparticles. Polym. Chem 5 (2014) 4032–4038.

[11]. Kim Y, Pyun J, Fréchet JMJ, Hawker CJ, Frank CW, The dramatic effect of architecture on the self-assembly of block copolymers at interfaces, Langmuir 21 (2005) 10444–10458. [PubMed: 16262305]

[12]. Zhou F, Xie M, Chen D, Structure and ultrasonic sensitivity of the superparticles formed by self-Assembly of single chain janus nanoparticles, Macromolecules 47 (2014) 365–372.

[13]. Wen J, Yuan L, Yang Y, Liu L, Zhao H, Self-assembly of monotethered single-chain nanoparticle shape amphiphiles, ACS Macro Lett 2 (2013) 100–106.

[14]. Zhang J, Tanaka J, Gurnani P, Wilson P, Hartlieb M, Perrier S, Self-assembly and disassembly of stimuli responsive tadpole-like single chain nanoparticles using a switchable hydrophilic/hydrophobic boronic acid cross-linker, Polym. Chem 8 (2017) 4079–4087.

[15]. Matsumoto M, Terashima T, Matsumoto K, Takenaka M, Sawamoto M, Compartmentalization technologies via self-assembly and cross-linking of amphiphilic random block copolymers in water, J. Am. Chem. Soc 139 (2017) 7164–7167. [PubMed: 28504881]

[16]. Wang J, Mao W, Lock LL, Tang J, Sui M, Sun W, Cui H, Xu D, Shen Y, The role of micelle size in tumor accumulation, penetration, and treatment, ACS Nano 9 (2015) 7195–7206. [PubMed: 26149286]

[17]. Peer D, Karp JM, Hong S, Farokhzad OC, Margalit R, Langer R, Nanocarriers as an emerging platform for cancer therapy, Nat. Nanotechnol 2 (2007) 751–760. [PubMed: 18654426]

[18]. Ju C, Mo R, Xue J, Zhang L, Zhao Z, Xue L, Ping Q, Zhang C, Sequential intra-intercellular nanoparticle delivery system for deep tumor penetration, Angew. Chem., Int. Ed 53 (2014) 6253–6258.

[19]. Jain RK, Stylianopoulos T, Delivering nanomedicine to solid tumors, Nat. Rev. Clin. Oncol 7 (2010) 653–664. [PubMed: 20838415]

[20]. Wong C, Stylianopoulos T, Cui J, Martin J, Chauhan VP, Jiang W, Popovic Z, Jain RK, Bawendi MG, Fukumura D, Multistage nanoparticle delivery system for deep penetration into tumor tissue, Proc. Natl. Acad. Sci. U.S 108 (2011) 2426–2431.

[21]. Kunjachan S, Pola R, Gremse F, Theek B, Ehling J, Moeckel D, Hermanns-Sachweh B, Pechar M, Ulbrich K, Hennink WE, Storm G, Lederle W, Kiessling F, Lammers T, Passive versus active tumor targeting using RGD- and NGR-modified polymeric nanomedicines, Nano Lett. 14 (2014) 972–981. [PubMed: 24422585]

[22]. Huang K, Ma H, Liu J, Huo S, Kumar A, Wei T, Zhang X, Jin S, Gan Y, Wang PC, He S, Zhang X, Liang XJ, Size-dependent localization and penetration of ultrasmall gold nanoparticles in cancer cells, multicellular spheroids, and tumors in vivo, ACS Nano 6 (2012) 4483–4493. [PubMed: 22540892]

[23]. Zhou C, Long M, Qin Y, Sun X, Zheng J, Luminescent gold nanoparticles with efficient renal clearance, Angew. Chem., Int. Ed 50 (2011) 3168–3172.

[24]. Miura Y, Takenaka T, Toh K, Wu S, Nishihara H, Kano M, Ino Y, Nomoto T, Matsumoto Y, Koyama H, Cabral H, Nishiyama N, Kataoka K, Cyclic RGD-linked polymeric micelles for targeted delivery of platinum anticancer drugs to glioblastoma through the blood–brain tumor barrier, ACS Nano 7 (2013) 8583–8592. [PubMed: 24028526]

[25]. Chen W, Su L, Zhang P, Li C, Zhang D, Wu W, Jiang X, Thermo and pH dual-responsive drug-linked pseudo-polypeptide micelles with a comb-shaped polymer as a micellar exterior, Polym. Chem 8 (2017) 6886–6894.

[26]. Lokerse WJM, Kneepkens ECM, ten Hagen TLM, Eggermont AMM, Grüll H, Koning GA, In depth study on thermosensitive liposomes: optimizing formulations for tumor specific therapy and in vitro to in vivo relations, Biomaterials 82 (2016) 138–150. [PubMed: 26761778]

[27]. Cheng W, Liang C, Xu L, Liu G, Gao N, Tao W, Luo L, Zuo Y, Wang X, Zhang X, Zeng X, Mei L, TPGS-functionalized polydopamine-modified mesoporous silica as drug nanocarriers for enhanced lung cancer chemotherapy against multidrug resistance, Small 13 (2017) 1700623.

[28]. Feng L, Gai S, He F, Dai Y, Zhong C, Yang P, Lin J, Multifunctional mesoporous ZrO2 encapsulated upconversion nanoparticles for mild NIR light activated synergistic cancer therapy, Biomaterials 147 (2017) 39–52. [PubMed: 28926732]

[29]. Wang S, Huang P, Chen X, Hierarchical targeting strategy for enhanced tumor tissue accumulation/retention and cellular internalization, Adv. Mater 28 (2016) 7340–7364. [PubMed: 27255214]

[30]. Heiden MGV, Cantley LC, Thompson CB, Understanding the warburg effect: the metabolic requirements of cell proliferation, Science 324 (2009) 1029–1033. [PubMed: 19460998]

[31]. Gatenby RA, Gillies RJ, Why do cancers have high aerobic glycolysis? Nat. Rev. Cancer 4 (2004) 891–899. [PubMed: 15516961]

[32]. Ghosh S, Basu S, Thayumanavan S, Simultaneous and reversible functionalization of copolymers for biological applications, Macromolecules 39 (2006) 5595–5597.

[33]. Friedrich J, Seidel C, Ebner R, Kunz-Schughart LA, Spheroid-based drug screen: considerations and practical approach, Nat. Protoc 4 (2009) 309–324. [PubMed: 19214182]

[34]. L. T, Gabrielson NP, Uckun FM, Fan TM, Cheng, Size-dependent tumor penetration and in vivo efficacy of monodisperse drug-silica nanoconjugates, Mol. Pharm 10 (2013) 883–892. [PubMed: 23301497]

[35]. Foster EJ, Berda EB, Meijer EW, Metastable supramolecular polymer nanoparticles via intramolecular collapse of single polymer chains, J. Am. Chem. Soc 131 (2009) 6964–6966. [PubMed: 19405473]

[36]. Murray BS, Fulton DA, Dynamic covalent single-chain polymer nanoparticles, Macromolecules 44 (2011) 7242–7252.

[37]. Zhang L, Eisenberg A, Multiple morphologies and characteristics of “crew-cut” micelle-like aggregates of polystyrene-b-poly(acrylic acid) diblock copolymers in aqueous solutions, J. Am. Chem. Soc 118 (1996) 3168–3181.

[38]. Zhang L, Shen H, Eisenberg A, Phase separation behavior and crew-cut micelle formation of polystyrene-b-poly(acrylic acid) copolymers in solutions, Macromolecules 30 (1997) 1001–1011.

[39]. Weaver JVM, Tang Y, Liu S, Iddon PD, Grigg R, Billingham NC, Armes SP, Hunter R, Rannard SP, Preparation of shell cross-linked micelles by polyelectrolyte complexation, Angew. Chem. Int. Ed 43 (2004) 1389–1392.

[40]. Fan J, Zeng F, Wu S, Wang X, Polymer micelle with pH-triggered hydrophobic-hydrophilic transition and de-cross-linking process in the core and its application for targeted anticancer drug delivery, Biomacromolecules 13 (2012) 4126–4137. [PubMed: 23145920]

[41]. Jiwpanich S, Ryu J-H, Bickerton S, Thayumanavan S, Non-covalent encapsulation stabilities in supramolecular nanoassemblies, J. Am. Chem. Soc 132 (2010)10683–10685. [PubMed: 20681699]

[42]. Lee MH, Sessler JL, Kim JS, Disulfide-based multifunctional conjugates for targeted theranostic drug delivery, Acc. Chem. Res 48 (2015) 2935–2946. [PubMed: 26513450]

[43]. Ryu J-H, Chacko RT, Jiwpanich S, Bickerton S, Babu RP, Thayumanavan S, Self-cross-linked polymer nanogels: a versatile nanoscopic drug delivery platform, J. Am. Chem. Soc 132 (2010) 17227–17235. [PubMed: 21077674]

[44]. Chauhan VP, Jain RK, Strategies for advancing cancer nanomedicine, Nat. Mater 12 (2013) 958–962. [PubMed: 24150413]

[45]. Perrault SD, Walkey C, Jennings T, Fischer HC, Chan WCW, Mediating tumor targeting efficiency of nanoparticles through design, Nano Lett. 9 (2009) 1909–1915. [PubMed: 19344179]

[46]. Sun Q, Sun X, Ma X, Zhou Z, Jin E, Zhang B, Shen Y, Van Kirk EA, Murdoch WJ, Lott JR, Lodge TP, Radosz M, Zhao Y, Integration of nanoassembly functions for an effective delivery cascade for cancer drugs, Adv. Mater 26 (2014) 7615–7621. [PubMed: 25328159]

[47]. Hühn D, Kantner K, Geidel C, Brandholt S, De Cock I, Soenen SJH, Gil PR, Montenegro J-M, Braeckmans K, Mullen K, Nienhaus GU, Klapper M, Parak WJ, Polymer-coated nanoparticles interacting with proteins and cells: focusing on the sign of the net charge, ACS nano 7 (2013) 3253–3263. [PubMed: 23566380]

[48]. Li L, Raghupathi K, Yuan C, Thayumanavan S, Surface charge generation in nanogels for activated cellular uptake at tumor-relevant pH, Chem. Sci 4 (2013) 3654–3660.

[49]. Zhang S, Li J, Lykotrafitis G, Bao G, Suresh S, Size-dependent endocytosis of nanoparticles, Adv. Mater 21 (2009) 419–424. [PubMed: 19606281]

[50]. Gao W, Yang X, Lin Z, He B, Mei D, Wang D, Zhang H, Zhang H, Dai W, Wang X, Zhang Q, The use of electronic-neutral penetrating peptides cyclosporin A to deliver pro-apoptotic peptide: a possibly better choice than positively charged TAT, J. Control. Release 261 (2017) 174–186. [PubMed: 28662902]

[51]. Nagy A, Steinbruck A, Gao J, Doggett N, Hollingsworth JA, Iyer R, Comprehensive analysis of the effects of CdSe quantum dot size, surface charge, and functionalization on primary human lung cells, ACS Nano 6 (2012) 4748–4762. [PubMed: 22587339]

[52]. Maeda H, Nakamura H, Fang J, The EPR effect for macromolecular drug delivery to solid tumors: improvement of tumor uptake, lowering of systemic toxicity, and distinct tumor imaging in vivo, Adv. Drug Deliv. Rev 65 (2013) 71–79. [PubMed: 23088862]

[53]. He C, Hu Y, Yin L, Tang C, Yin C, Effects of particle size and surface charge on cellular uptake and biodistribution of polymeric nanoparticles, Biomaterials 31 (2010) 3657–3666. [PubMed: 20138662]

[54]. Lee JS, Ankone M, Pieters E, Schiffelers RM, Hennink WE, Feijen J, Circulation kinetics and biodistribution of dual-labeled polymersomes with modulated surface charge in tumor-bearing mice: comparison with stealth liposomes, J. Control. Release 155 (2011) 282–288. [PubMed: 21820023]

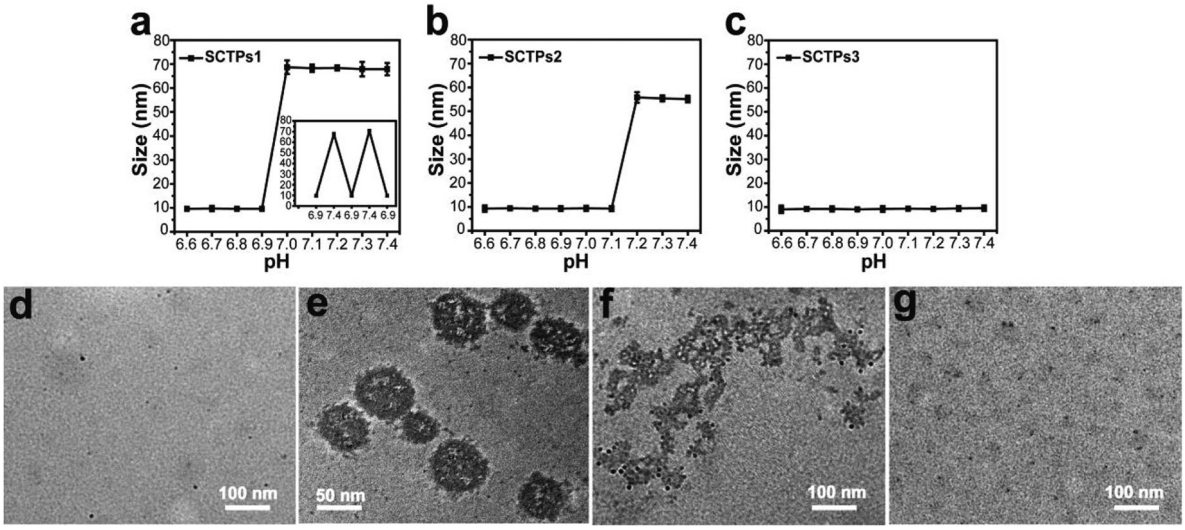

Fig. 1.

pH-dependent size change. (a) **SCTPs1**, the inset is the size variation of **SCTPs1** with pH, (b) **SCTPs2**, and (c) **SCTPs3** analysed by DLS. TEM of the assembly and dissociation, (d) **SCTPs1**, (e) MTAs, assembled by **SCTPs1** at pH 7.4, (f) **SCTPs1**, dissociating from MTAs, and (g) complete dissociation at pH 6.9. TEM samples were stained with RuO_4.

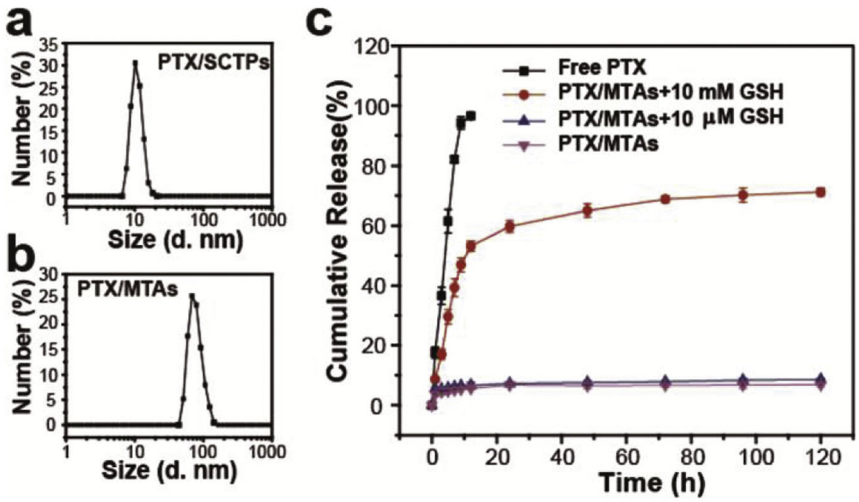

Fig. 2.

DLS of (a) PTX/SCTPs and (b) PTX/MTAs. (c) *In vitro* PTX release in PBS of pH 6.9 containing 0.2% (w/v) Tween 80 at 37 °C.

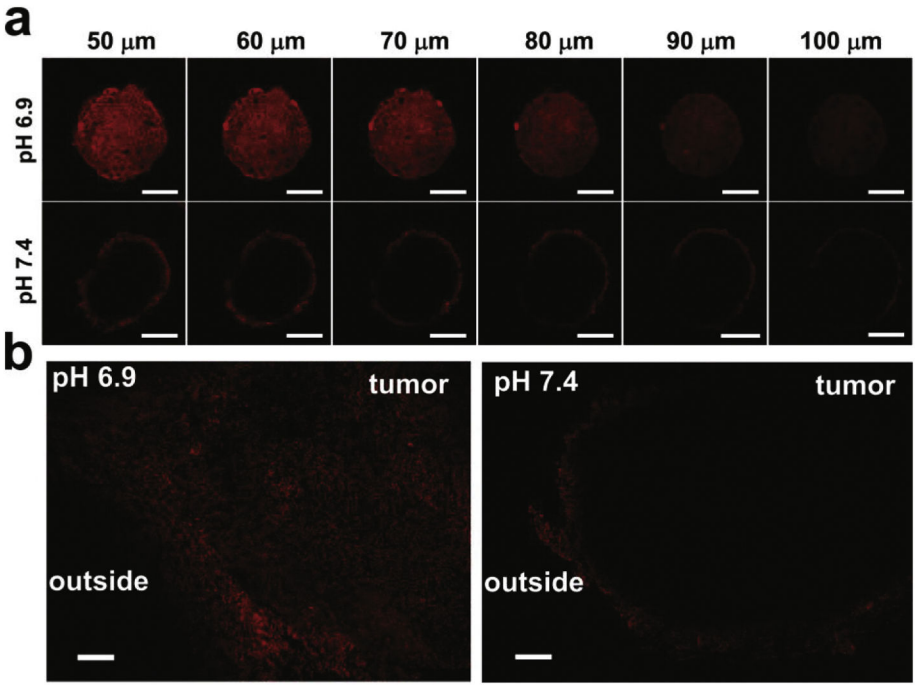

Fig. 3.

(a) CLSM images of MCTS for the *ex vivo* penetrating test. The MCTS were incubated with $^{Cy5.5}$MTAs for 4 h at pH 6.9 and 7.4, and measured by CLSM Z-stack scanning. Scale bar: 200 μm. (b) Fluorescence images of the slides sectioned from the treated 4T1 tumors. The tumors were cultured for 24 h in the presence of $^{Cy5.5}$MTAs in medium adjusted to pH 6.9 and 7.4. Scale bar: 200 μm.

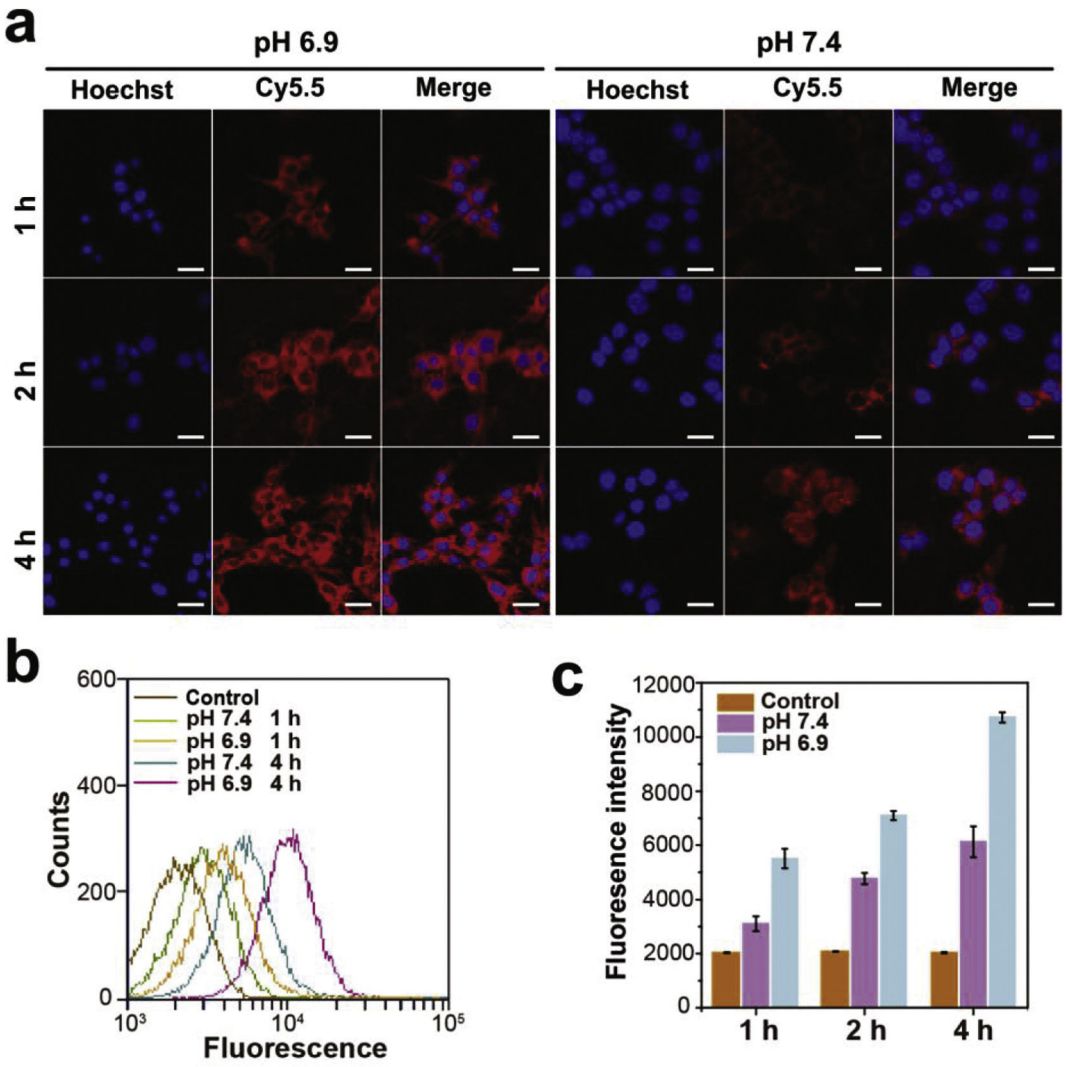

Fig. 4.

(a) CLSM images and (b) flow cytometry data of 4T1 cells incubated with $^{Cy5.5}$MTAs at pH 6.9 and 7.4. Scale bar: 25 μm. (c) The fluorescence intensity of Cy 5.5 accumulation at designed time.

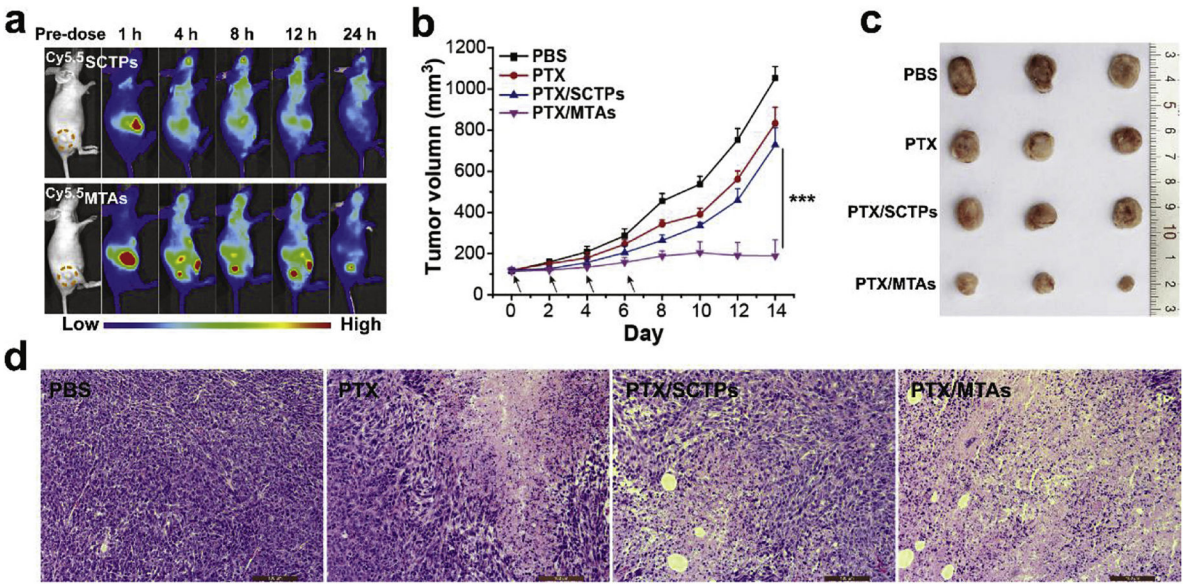

Fig. 5.

(a) *In vivo* fluorescence images of 4T1 tumor-bearing nude mice taken at 1, 4, 8, 12, and 24 h after intravenous injection of $^{Cy5.5}$SCTPs and $^{Cy5.5}$MTAs. (b) Tumor growth curves of mice during the treatment with PBS, PTX, PTX/SCTPs, and PTX/MTAs. Statistical significance: ***$p < 0.001$. (c) Photograph of tumors collected from different groups at the end of treatment. (d) H&E stained tumor slices after treatment. Scale bar: 100 μm.

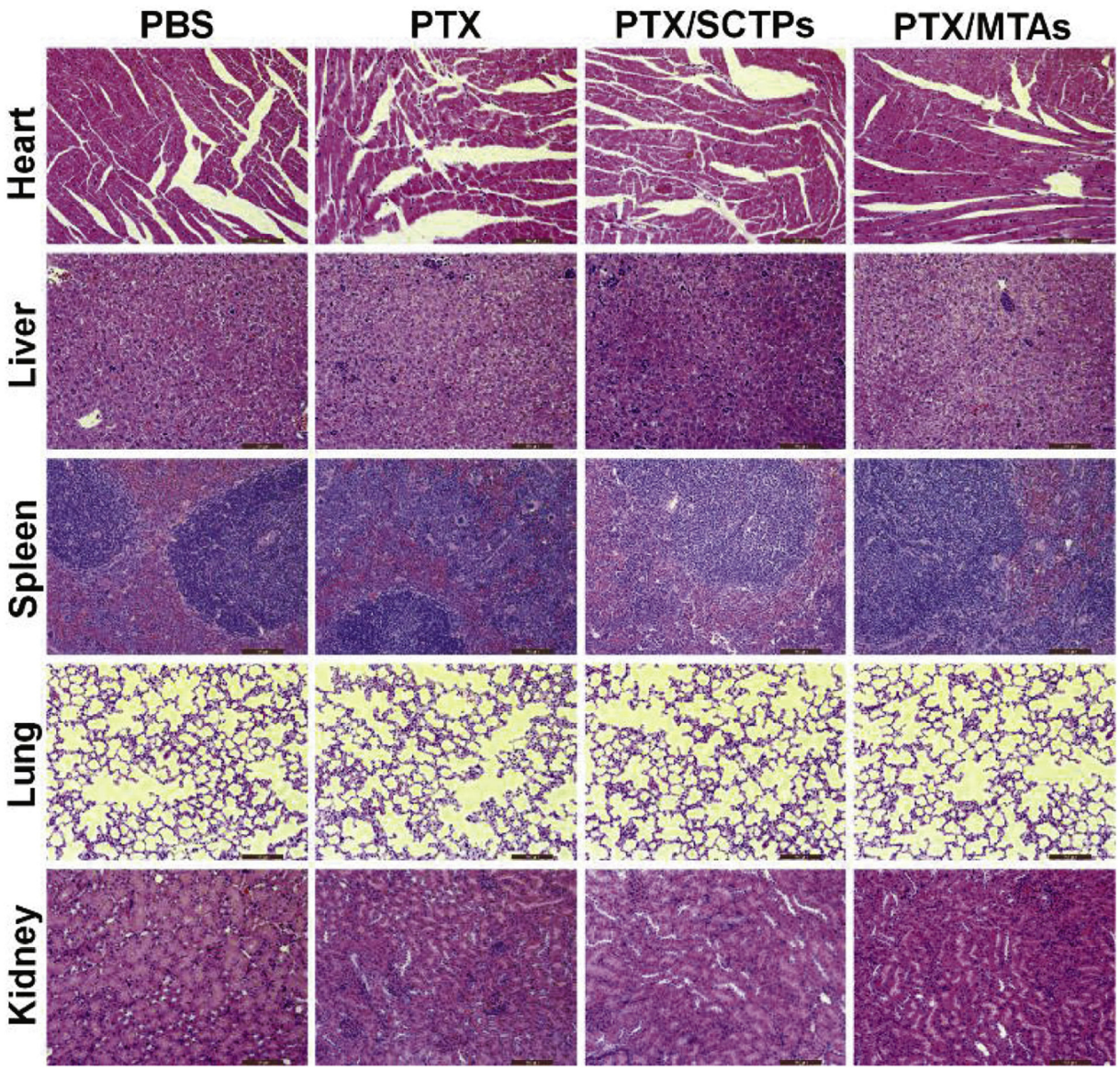

Fig. 6.

H&E stained heart, liver, spleen, lung, and kidney from the mice after treatment. Scale bar: 100 μm.

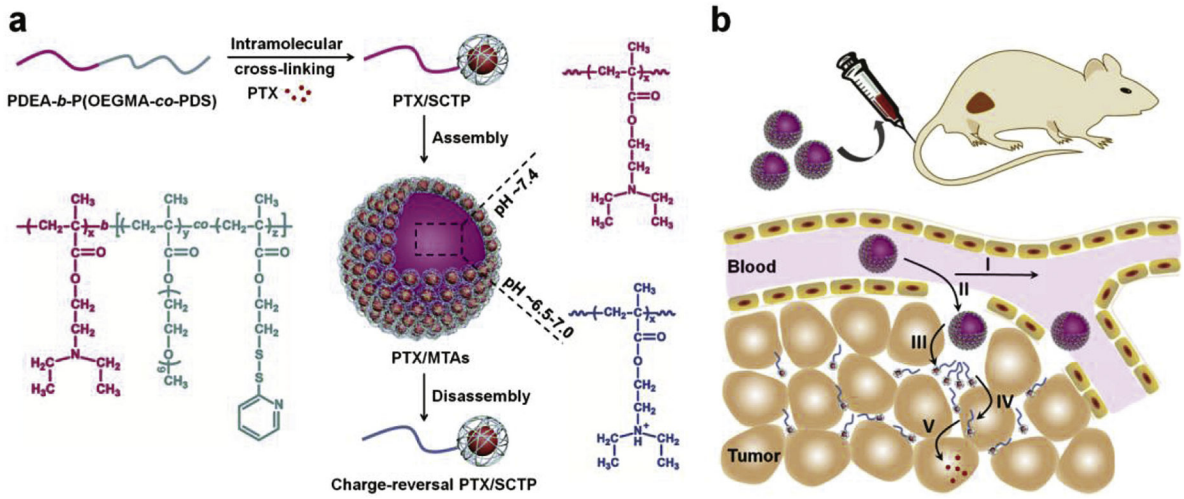

Scheme 1.

(a) Illustration of the preparation of PTX/MTAs from PDEA-*b*-P(OEGMA-*co*-PDS) copolymer and the pH-sensitive morphological transition. (b) Schematic illustration of delivery cascade of PTX/MTAs. I) Circulation in the blood vessel; II) Extravasation into tumor; III) PTX/SCTPs dissociating from PTX/MTAs and penetrating into tumor tissue; IV) PTX/SCTPs becoming positively charged as the acidity increase and expediting the cellular uptake; V) Intracellular drug release in respond to a redox stimulus.

Table 1.

Characteristics of $PDEA_x$-*b*-$P(OEGMA_y$-*co*-$PDS_z)$

Sample	x/y/z [a]	M_n [b] (kDa)	PDI [b]
P1	78/80/32	33.2	1.15
P2	52/81/32	29.8	1.14
P3	28/78/31	24.9	1.19

[a] Calculated by ^{1}H NMR.

[b] Determined by GPC in DMF using PMMA as standards.